

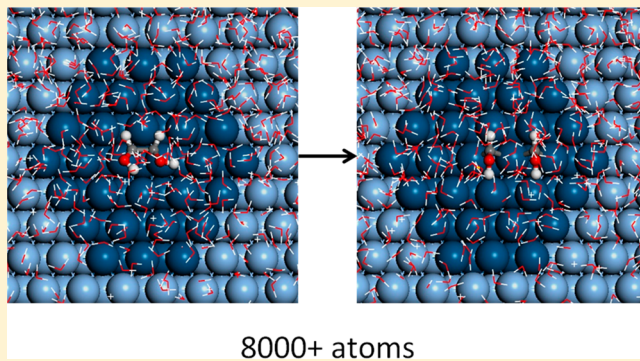
Hybrid Quantum Mechanics/Molecular Mechanics Solvation Scheme for Computing Free Energies of Reactions at Metal–Water Interfaces

Muhammad Faheem and Andreas Heyden*

Department of Chemical Engineering, University of South Carolina, 301 South Main Street, Columbia, South Carolina 29208, United States

S Supporting Information

ABSTRACT: We report the development of a quantum mechanics/molecular mechanics free energy perturbation (QM/MM-FEP) method for modeling chemical reactions at metal–water interfaces. This novel solvation scheme combines planewave density function theory (DFT), periodic electrostatic embedded cluster method (PEECM) calculations using Gaussian-type orbitals, and classical molecular dynamics (MD) simulations to obtain a free energy description of a complex metal–water system. We derive a potential of mean force (PMF) of the reaction system within the QM/MM framework. A fixed-size, finite ensemble of MM conformations is used to permit precise evaluation of the PMF of QM coordinates and its gradient defined within this ensemble. Local conformations of adsorbed reaction moieties are optimized using sequential MD-sampling and QM-optimization steps. An approximate reaction coordinate is constructed using a number of interpolated states and the free energy difference between adjacent states is calculated using the QM/MM-FEP method. By avoiding on-the-fly QM calculations and by circumventing the challenges associated with statistical averaging during MD sampling, a computational speedup of multiple orders of magnitude is realized. The method is systematically validated against the results of ab initio QM calculations and demonstrated for C–C cleavage in double-dehydrogenated ethylene glycol on a Pt (111) model surface.



1. INTRODUCTION

Computational investigations of chemical reactions at solid–liquid interfaces have long been and continue to be very challenging. Liquid molecules can affect the activity and selectivity of a heterogeneous catalyst in a variety of ways. Long-range electrostatic interactions of solvent molecules with other solvent molecules and with the catalyst and the adsorbed moieties create a reaction environment that is radically different from the gas phase, resulting in stabilization or destabilization of charged intermediates and transition states.¹ Nonharmonic dynamic fluctuations in a complex liquid phase and diffusion of the solvent molecules can affect reactant and product diffusivities² and alter the dynamics of energy accumulation and relaxation. Direct participation of solvent molecules in the reaction mechanism not only causes a concentration effect on the overall rate of reaction but can also provide lower-energy pathways, for example, for proton transfer between neighboring active sites.³ Solute–solvent phase equilibria can affect the overall selectivity by suppressing or enhancing various reaction pathways.⁴ Reaction free energies, free energy barriers, and turnover frequencies of elementary reaction steps occurring at a solid–liquid interface can therefore be very different from when the same processes occur at a solid–gas interface.⁵ Unfortunately, due to a lack of a well-established methodology for describing the influence of dynamic fluctuations of the liquid

phase on chemical reactions across a solid–liquid interface with quantum mechanical (QM) accuracy, we have currently only a limited understanding of the structure–activity relationships of heterogeneous catalysts in liquid phase and we are unable to rationally design new catalytic materials for liquid phase processes.

Computer simulations of chemical reactions at solid–liquid interfaces face multiple challenges. First, the potential energy surface (PES) must accurately describe the electronic structure of the most interesting part of the system directly involved in the bond forming or breaking process, that is, the active site of the catalyst, adsorbed moiety, and possibly some solvent molecules in the immediate neighborhood. Second, a significant fraction of the system configuration space must be sampled for calculation of accurate free energy differences and to ensure that the results are statistically converged. Finally, nonharmonic dynamic fluctuations in the liquid phase, long-range electrostatic interactions between water molecules, delocalization of electrons in transition metals, and finite size effects^{6,7} all require the computational model to be sufficiently large. Although ab initio molecular dynamics (AIMD) approaches⁸ can, in principle, be used for such simulations, current computer

Received: March 12, 2014

Published: May 28, 2014



ACS Publications

© 2014 American Chemical Society

3354

dx.doi.org/10.1021/ct500211w | J. Chem. Theory Comput. 2014, 10, 3354–3368

technology and resources limit a full quantum mechanical treatment of the entire condensed-phase reaction system to a few hundred atoms and a few picoseconds of simulation time.^{9–11} This necessitates the development of alternative computational approaches that are nearly as accurate as AIMD but computationally multiple (5–7) orders of magnitude less expensive.

One approach that circumvents these problems is the use of isotropic continuum solvation models.^{12,13} The solvent is modeled as a homogeneous medium characterized by an appropriate dielectric constant, and the solute is placed in carefully constructed cavities within this continuum.¹⁴ QM charge distribution of the solute polarizes the surrounding dielectric medium. The response of the polarized solvent creates a reaction field which is included as electrostatic potential (ESP) in the self-consistent field (SCF) calculations at the same level of QM theory. Implicit solvation models are computationally very efficient because, in the absence of explicit solvent molecules, the size of the electronic structure problem is the same as in gas phase. This approach has been used to study the formation of water on Pt and Pt-based alloys¹⁵ and the oxidation of formic acid at the Pt/H₂O interface.¹⁶ Recently, we have developed the iSMS¹⁷ (Implicit Solvation for Metal Surfaces) method for combining nonperiodic implicit solvation models with planewave density functional theory (DFT) calculations to describe the effect of solvents on processes occurring at “periodic” metal–water interfaces. This method has been successfully applied for calculating CO frequency shifts on Pd/H₂O and Pt/H₂O interfaces¹⁷ and for predicting solvent effects on the hydrodeoxygenation of propanoic acid over Pd (111).¹⁸ Although implicit solvation models are generally reasonably accurate for computing free energies in solution, they cannot correctly reproduce the anisotropic site-specific interactions¹⁹ between the solute and solvent molecules over a solid catalyst. Inclusion of one or more explicit solvent molecules as part of the QM solute structure may help in some cases,¹⁶ but the broader challenge of sampling the configuration space of a complex liquid environment in a statistically relevant manner remains unaddressed.

An alternative approach based on ab initio QM calculations consists of optimizing a hexagonally close-packed ice-like network of water molecules^{20,21} at the metal interface before replacing one of the water molecules with a reaction moiety. The preoptimized water network effectively serves as an initial guess for further geometry optimizations and transition state searches. This approach has been used to study methanol decomposition on Pt (111)²² and selective oxidation of ethanol to acetic acid on Pt (111) and Au (111).²³ However, such “freezing” of the water structure leads to insufficient sampling of the water configuration space and the predicted adsorption energies and activation barriers are often highly dependent on the initial structure guess. A more suitable approach would be to perform such optimizations in an average field of a sufficiently large number of water conformations. This is, however, impossible with ab initio methods for the foreseeable future.

The dual need for both accurate electronic structure calculations and extensive configuration space sampling is not unique for reactions at metal–water interfaces. A similar problem is encountered in modeling enzyme-catalyzed processes and molecular biological systems where the system of interest often contains tens of thousands to millions of

atoms. A closer examination reveals that, in many chemical reactions, bond breaking and forming are localized events and involve relatively few atoms. The interactions of these “active” atoms must be described accurately. Atoms in the remainder of the system experience minimal changes in their electronic structures but still contribute to the reaction process by creating a unique steric and electrostatic environment around the active site. This permits the use of multilevel quantum mechanical/molecular mechanical (QM/MM) methods²⁴ where only the active site of, for example, the enzyme and its immediate environment, that make the most important and direct contributions to the electronic structure of the atoms involved in reaction chemistry, are described quantum mechanically, whereas the remainder of the system, for example, the nonreactive part of the enzyme and the bulk of the liquid water, is treated at classical molecular mechanical level of theory. This combination of a moderately sized QM region and a large classical MM region provides an accurate yet computationally affordable energetic description of the complex system. Similar arguments can be made for metal-catalyzed reactions in water. For most reaction moieties, the adsorption site involves a handful of metal atoms. Metal–water interactions only involve a limited amount of charge transfer that is localized at the interface.²⁵ In addition, we have recently shown that the effect of water on the bonding characteristics of transition metal surfaces with adsorbates is short-ranged in metal.¹⁷ Noting that the enzyme catalysis community has developed various highly efficient QM/MM algorithms for calculating reaction free energies and free energy barriers,^{26–30} we hypothesize that it is possible to develop similar approaches for simulating chemical reactions at metal–water interfaces.

In this paper, we report the development of a hybrid QM/MM methodology, named eSMS (Explicit Solvation for Metal Surfaces), for modeling reactions at metal–water interfaces. The proposed procedure has similarity to our recently developed iSMS method but uses an all atom description of the reaction system, involves QM/MM-FEP (free energy perturbation)³¹ calculations and can therefore be considered as a bridge between implicit solvation models and AIMD approaches. The objective of this theoretical study is to validate this procedure for a model C–C cleavage reaction at the Pt (111)/H₂O interface. This paper is organized as follows: In section 2, we first introduce our QM/MM approach and derive an expression for the total QM/MM energy with approximate QM/MM electrostatic interactions. We then derive an equivalent but more practical expression that permits easier integration of various QM and MD program packages. Next, we derive expressions for the potential of mean force (PMF) of QM coordinates and its gradient within the QM/MM-FEP framework and show how these results can be integrated with our eSMS method in a step-by-step procedure. Computational details are outlined in section 3 and comprehensive results addressing the validation and application of the proposed methodology are presented in section 4. Finally, general conclusions of this work are summarized in section 5.

2. THEORY

2.1. Approximate Total QM/MM Energy Function.

In the combined QM/MM approach, the model system is partitioned into QM (r_{QM}) and MM (r_{MM}) subsystems. Each atom of the entire system is assigned to either of the subsystems. Because of the interaction between the two subsystems, the total QM/MM energy is not simply a sum of

the energies of the individual subsystems, but must also include their interaction energy. In general,³² the total energy of the system (E_T) can be written as

$$\begin{aligned} E_T(\underline{r}_{QM}, \underline{r}_{MM}) &= E_{QM}(\underline{r}_{QM}) + E_{QM/MM}(\underline{r}_{QM}, \underline{r}_{MM}) \\ &+ E_{MM}(\underline{r}_{MM}) \end{aligned} \quad (1)$$

The three terms on the right-hand side are the energy of the QM subsystem (E_{QM}), the interaction energy between the QM and MM subsystems ($E_{QM/MM}$), and the energy of the MM subsystem (E_{MM}), respectively. Equation 1 is the working equation adopted in the majority of QM/MM schemes³² and carries no assumption as long as the selected QM and MM methods are capable of describing the respective subsystems and their interaction. The QM/MM interaction energy can be further decomposed into electrostatic ($E_{QM/MM}^{elec}$), van der Waals ($E_{QM/MM}^{vdW}$), and covalent ($E_{QM/MM}^{cov}$) contributions. For simulating elementary processes at metal–water interfaces, we define a QM subsystem containing some metal atoms, adsorbed reaction moieties, and possibly a few water molecules, whereas the MM subsystem contains only water molecules and metal atoms far away from the reaction site. Since there are no covalent bonds connecting the QM and MM subsystems in our problems of interest (there are only metallic bonds), this partitioning scheme considerably simplifies the description of the boundary between the two subsystems and as we will show below, eliminates the need to consider alternative approaches, for example, adding link hydrogen atoms,³³ pseudo-bond method,³⁴ or the frozen local-orbital method.³⁵

$$\begin{aligned} E_T(\underline{r}_{QM}, \underline{r}_{MM}) &= E_{QM}(\underline{r}_{QM}) + E_{QM/MM}^{elec}(\underline{r}_{QM}, \underline{r}_{MM}) \\ &+ E_{QM/MM}^{vdW}(\underline{r}_{QM}, \underline{r}_{MM}) + E_{MM}(\underline{r}_{MM}) \end{aligned} \quad (2)$$

Using an electrostatic embedding scheme, the electrostatic potential (ESP) from the MM atoms can be rigorously included in the QM calculations at the same level of theory, allowing the QM energy (E_{QM}) and QM/MM electrostatic interaction energy ($E_{QM/MM}^{elec}$) to be computed together in a self-consistent manner.

$$\begin{aligned} E_{QM}(\underline{r}_{QM}) + E_{QM/MM}^{elec}(\underline{r}_{QM}, \underline{r}_{MM}) \\ = \langle \Psi | H_{eff}(\underline{r}_{QM}, \underline{r}_{MM}) | \Psi \rangle \end{aligned} \quad (3)$$

$$\begin{aligned} E_T(\underline{r}_{QM}, \underline{r}_{MM}) &= \langle \Psi | H_{eff}(\underline{r}_{QM}, \underline{r}_{MM}) | \Psi \rangle \\ &+ E_{QM/MM}^{vdW}(\underline{r}_{QM}, \underline{r}_{MM}) + E_{MM}(\underline{r}_{MM}) \end{aligned} \quad (4)$$

Here, H_{eff} is the effective QM Hamiltonian which includes the electrostatic potential of the MM subsystem, and Ψ is the electronic wave function of the QM subsystem. Computation of this wave function is the bottleneck for application of eq 4 since a new SCF calculation is required for each QM or MM conformation. To address this problem, we consider the reaction path potential (RPP) method developed by Lu and Yang.³⁶ The idea is to separate the QM energy into two components that can be expanded analytically in terms of both changes in the QM conformation and the MM electrostatic potential. We assume that the QM/MM electrostatic interaction can be approximated as the Coulombic interactions between MM point charges and ESP-fitted charges on the QM atoms.

$$E_{QM/MM}^{elec(ESP)}(\underline{r}_{QM}, \underline{r}_{MM}) = \sum_{j \in MM} \sum_{i \in QM} \frac{q_j Q_i(\underline{r}_{QM}, \underline{r}_{MM})}{|\underline{r}_{QM,i} - \underline{r}_{MM,j}|} \quad (5)$$

Here, q_j is the point charge of MM atom j from the MM force field which is usually a constant. The ESP-fitted charge of QM atom i , $Q_i(\underline{r}_{QM}, \underline{r}_{MM})$, depends on all QM and MM coordinates in the system. Next, we define a QM internal energy function³⁶ (E'_{QM}) as the energy of the QM subsystem in the presence of an electrostatic field of MM point charges, minus the Columbic interactions between MM point charges and ESP-fitted charges of QM atoms.

$$\begin{aligned} E'_{QM}(\underline{r}_{QM}, \underline{r}_{MM}) &\equiv \langle \Psi | H_{eff}(\underline{r}_{QM}, \underline{r}_{MM}) | \Psi \rangle \\ &- E_{QM/MM}^{elec(ESP)}(\underline{r}_{QM}, \underline{r}_{MM}) \end{aligned} \quad (6)$$

Equation 4 can now be written as

$$\begin{aligned} E_T(\underline{r}_{QM}, \underline{r}_{MM}) &= E'_{QM}(\underline{r}_{QM}, \underline{r}_{MM}) \\ &+ \sum_{j \in MM} \sum_{i \in QM} \frac{q_j Q_i(\underline{r}_{QM}, \underline{r}_{MM})}{|\underline{r}_{QM,i} - \underline{r}_{MM,j}|} + E_{QM/MM}^{vdW} \\ &(\underline{r}_{QM}, \underline{r}_{MM}) + E_{MM}(\underline{r}_{MM}) \end{aligned} \quad (7)$$

Calculation of E'_{QM} also requires a new SCF calculation for each QM or MM conformation. For configuration space sampling in long-time MD simulations, it is highly desirable to reformulate eq 7 as an approximate total QM/MM energy function without the need for recurrent SCF calculations.

In this context, perturbation theory can be used where changes in the total energy of the system, for a given QM conformation, are characterized by the response to changes in electrostatic potential of the MM atoms. Although expressions for higher-order perturbations are available,^{36–39} we limit our approach to a zero-order approximation, assuming that it is adequate to neglect changes in polarization of the QM subsystem in response to moving MM atoms in the environment. In other words, both QM conformation and QM electron density are frozen during MD simulations.^{29,37} Using a reference MM conformation \underline{r}_{MM}^0

$$\begin{aligned} Q_i(\underline{r}_{QM}, \underline{r}_{MM}) &\approx Q_i(\underline{r}_{QM}, \underline{r}_{MM}^0) \\ E_{QM/MM}^{elec(ESP)}(\underline{r}_{QM}, \underline{r}_{MM}) &= \sum_{j \in MM} \sum_{i \in QM} \frac{q_j Q_i(\underline{r}_{QM}, \underline{r}_{MM})}{|\underline{r}_{QM,i} - \underline{r}_{MM,j}|} \\ &\approx \sum_{j \in MM} \sum_{i \in QM} \frac{q_j Q_i(\underline{r}_{QM}, \underline{r}_{MM}^0)}{|\underline{r}_{QM,i} - \underline{r}_{MM,j}|} \end{aligned} \quad (8)$$

$$\begin{aligned} E'_{QM}(\underline{r}_{QM}, \underline{r}_{MM}) &\approx E'_{QM}(\underline{r}_{QM}, \underline{r}_{MM}^0) \\ &= \langle \Psi | H_{eff}(\underline{r}_{QM}, \underline{r}_{MM}^0) | \Psi \rangle \\ &- \sum_{j \in MM} \sum_{i \in QM} \frac{q_j Q_i(\underline{r}_{QM}, \underline{r}_{MM}^0)}{|\underline{r}_{QM,i} - \underline{r}_{MM,j}|} \end{aligned} \quad (9)$$

With these assumptions, the approximate total QM/MM energy (\tilde{E}_T) is written using eq 7.

$$\begin{aligned}\tilde{E}_T(\underline{r}_{QM}, \underline{r}_{MM}) &= \langle \Psi | H_{eff}(\underline{r}_{QM}, \underline{r}_{MM}^0) | \Psi \rangle \\ &- \sum_{j \in MM} \sum_{i \in QM} \frac{q_j Q_i(\underline{r}_{QM}, \underline{r}_{MM}^0)}{|\underline{r}_{QM,i} - \underline{r}_{MM,j}^0|} \\ &+ \sum_{j \in MM} \sum_{i \in QM} \frac{q_j Q_i(\underline{r}_{QM}, \underline{r}_{MM}^0)}{|\underline{r}_{QM,i} - \underline{r}_{MM,j}|} + E_{QM/MM}^{vdW} \\ &(\underline{r}_{QM}, \underline{r}_{MM}) + E_{MM}(\underline{r}_{MM})\end{aligned}\quad (10)$$

We note here that the Coulombic interaction term describing $E_{QM/MM}^{elec(ESP)}$ is included in eq 10 twice in different contexts. First, it is subtracted as a constant evaluated at the reference MM conformation; then it is added for all MM conformations assuming constant ESP charges for the QM atoms (evaluated at the reference MM conformation).

2.2. Alternative Expression for the Approximate Total QM/MM Energy Function.

When the QM and MM calculations are performed using different program packages, there is a need to streamline the communication and exchange of information between them. In the following, we derive an equivalent but more practical expression for the approximate total QM/MM energy function. As described earlier, an electrostatic embedding scheme will be used to calculate both the energy of the QM subsystem and the QM/MM electrostatic interactions in a self-consistent manner. However, in most program packages these calculations do not include the electrostatic and van der Waals interactions within the MM subsystem and the van der Waals interactions between the QM and MM subsystems. All these contributions must be included with the MM program package. The total energy of the QM/MM system in a reference MM conformation can be expressed as

$$\begin{aligned}E_T(\underline{r}_{QM}, \underline{r}_{MM}^0) &= \langle \Psi | H_{eff}(\underline{r}_{QM}, \underline{r}_{MM}^0) | \Psi \rangle + E_{MM}^{elec}(\underline{r}_{MM}^0) \\ &+ E_{MM+QM/MM}^{vdW}(\underline{r}_{QM}, \underline{r}_{MM}^0)\end{aligned}\quad (11)$$

where we neglected for simplicity all intramolecular force field contributions in the MM subsystem because they are not present in most water force field models. Adding these intramolecular contributions for any solvent model does not add any complication as long as the QM/MM interface does not cross chemical bonds.

Substituting eq 6 in eq 11 and noting that ESP charges are required only for QM atoms whereas point charges for MM atoms are obtained from the force field

$$\begin{aligned}E_T(\underline{r}_{QM}, \underline{r}_{MM}^0) &= E'_{QM}(\underline{r}_{QM}, \underline{r}_{MM}^0) + E_{MM+QM/MM}^{elec(ESP)} \\ &(\underline{r}_{QM}, \underline{r}_{MM}^0) + E_{MM+QM/MM}^{vdW}(\underline{r}_{QM}, \underline{r}_{MM}^0)\end{aligned}\quad (12)$$

Similarly, for any other MM conformation

$$\begin{aligned}E_T(\underline{r}_{QM}, \underline{r}_{MM}) &= E'_{QM}(\underline{r}_{QM}, \underline{r}_{MM}) + E_{MM+QM/MM}^{elec(ESP)} \\ &(\underline{r}_{QM}, \underline{r}_{MM}) + E_{MM+QM/MM}^{vdW}(\underline{r}_{QM}, \underline{r}_{MM})\end{aligned}\quad (13)$$

Subtracting eq 12 from eq 13

$$\begin{aligned}\tilde{E}_T(\underline{r}_{QM}, \underline{r}_{MM}) - E_T(\underline{r}_{QM}, \underline{r}_{MM}^0) &= E'_{QM}(\underline{r}_{QM}, \underline{r}_{MM}) \\ &- E'_{QM}(\underline{r}_{QM}, \underline{r}_{MM}^0) + E_{MM+QM/MM}^{elec(ESP)}(\underline{r}_{QM}, \underline{r}_{MM}) \\ &- E_{MM+QM/MM}^{elec(ESP)}(\underline{r}_{QM}, \underline{r}_{MM}^0) + E_{MM+QM/MM}^{vdW} \\ &(\underline{r}_{QM}, \underline{r}_{MM}) - E_{MM+QM/MM}^{vdW}(\underline{r}_{QM}, \underline{r}_{MM}^0)\end{aligned}\quad (14)$$

Making the approximation of an invariant QM internal energy function as in eq 9, the first two terms on the right-hand side of eq 14 cancel each other. In addition, assumption of invariant polarization of QM atoms (eq 8) means that the electrostatic interactions within the QM subsystem will be exactly same for all MM conformations.

$$\begin{aligned}Q_i(\underline{r}_{QM}, \underline{r}_{MM}) &\approx Q_i(\underline{r}_{QM}, \underline{r}_{MM}^0) \\ E_{QM}^{elec(ESP)}(\underline{r}_{QM}) &= E_{QM}^{elec(ESP)}(\underline{r}_{QM}, \underline{r}_{MM}) \\ &= E_{QM}^{elec(ESP)}(\underline{r}_{QM}, \underline{r}_{MM}^0) = \text{constant}\end{aligned}\quad (15)$$

With these assumptions, eq 14 is rewritten as

$$\begin{aligned}\tilde{E}_T(\underline{r}_{QM}, \underline{r}_{MM}) - E_T(\underline{r}_{QM}, \underline{r}_{MM}^0) &= E_{QM}^{elec(ESP)}(\underline{r}_{QM}, \underline{r}_{MM}) - E_{QM}^{elec(ESP)}(\underline{r}_{QM}, \underline{r}_{MM}^0) \\ &- E_{MM+QM/MM}^{elec(ESP)}(\underline{r}_{QM}, \underline{r}_{MM}) + E_{MM+QM/MM}^{elec(ESP)}(\underline{r}_{QM}, \underline{r}_{MM}^0) \\ &+ E_{MM+QM/MM}^{vdW}(\underline{r}_{QM}, \underline{r}_{MM}) - E_{MM+QM/MM}^{vdW}(\underline{r}_{QM}, \underline{r}_{MM}^0) \\ &(\underline{r}_{QM}, \underline{r}_{MM}^0)\end{aligned}\quad (16)$$

Combining terms that can be computed together

$$\begin{aligned}\tilde{E}_T(\underline{r}_{QM}, \underline{r}_{MM}) - E_T(\underline{r}_{QM}, \underline{r}_{MM}^0) &= E_{QM+MM+QM/MM}^{elec(ESP)+vdW} \\ &(\underline{r}_{QM}, \underline{r}_{MM}) - E_{QM+MM+QM/MM}^{elec(ESP)+vdW}(\underline{r}_{QM}, \underline{r}_{MM}^0)\end{aligned}\quad (17)$$

where $E_{QM+MM+QM/MM}^{elec(ESP)+vdW}(\underline{r}_{QM}, \underline{r}_{MM})$ is the energy of the total system at the MM level of theory. We note that the electrostatic and van der Waals interactions of the QM subsystem cancel on the right side of eq 17 due to an identical QM geometry and the frozen charge approximation. Finally, substituting eq 11 in eq 17 and rearranging

$$\begin{aligned}\tilde{E}_T(\underline{r}_{QM}, \underline{r}_{MM}) &= \langle \Psi | H_{eff}(\underline{r}_{QM}, \underline{r}_{MM}^0) | \Psi \rangle + E_{MM}^{elec}(\underline{r}_{MM}^0) \\ &+ E_{MM+QM/MM}^{vdW}(\underline{r}_{QM}, \underline{r}_{MM}^0) + E_{QM+MM+QM/MM}^{elec(ESP)+vdW}(\underline{r}_{QM}, \underline{r}_{MM}) \\ &- E_{QM+MM+QM/MM}^{elec(ESP)+vdW}(\underline{r}_{QM}, \underline{r}_{MM}^0)\end{aligned}\quad (18)$$

The second and third terms on right-hand side can be combined by removing charges from all QM atoms in their evaluation.

$$\begin{aligned}\tilde{E}_T(\underline{r}_{QM}, \underline{r}_{MM}) &= \langle \Psi | H_{eff}(\underline{r}_{QM}, \underline{r}_{MM}^0) | \Psi \rangle \\ &+ [E_{MM+QM/MM}^{elec+vdW}(\underline{r}_{QM}, \underline{r}_{MM}^0)]_{Q_i=0, i \in QM} \\ &+ E_{QM+MM+QM/MM}^{elec(ESP)+vdW}(\underline{r}_{QM}, \underline{r}_{MM}) \\ &- E_{QM+MM+QM/MM}^{elec(ESP)+vdW}(\underline{r}_{QM}, \underline{r}_{MM}^0)\end{aligned}\quad (19)$$

Evaluation of $\tilde{E}_T(\underline{r}_{QM}, \underline{r}_{MM})$ using eq 19 thus requires one SCF calculation in the electrostatic potential of the reference MM conformation to obtain the QM internal energy and ESP-fitted charges for the QM atoms, one MM calculation for each MM conformation where all QM atoms are assigned ESP-fitted charges, and one additional MM calculation for the reference

MM conformation where charges from all QM atoms have been removed.

Equation 19 is a general formulation for the approximate total QM/MM energy function for MM subsystems with no intramolecular interactions and a QM/MM interface that does not cross chemical bonds. Addition of intramolecular interactions to the MM subsystem is trivial. The significance of this formulation is that it allows interfacing of any combination of QM and MM program packages through simple file parsers without modifying the respective source codes.

2.3. Potential of Mean Force of QM Coordinates. For a complex metal–water interface model, the enormous number of water degrees of freedom makes it virtually impossible to explore the full potential energy landscape with high accuracy (QM level of theory). Even if high level QM calculations were possible for such complex systems, insufficient sampling due to the finite length and time scales of currently practical simulations would impede calculation of accurate free energies. Instead, one can focus on a potential of mean force (PMF) description of the reaction system in terms of the most important degrees of freedom where contributions from less important degrees of freedom are ensemble-averaged. While solvent/water coordinates can be included in the reaction coordinate, we limit ourselves here to reaction coordinates that do not include water coordinates. As a result, the PMF is an approximation for the free energy of the QM/MM system under the mean-field and frozen QM approximation.³⁷

In order to derive a PMF description with respect to QM coordinates, we recall that the total partition function of the QM/MM system is

$$Z_T = \int \exp\{-\beta E_T(\underline{r}_{QM}, \underline{r}_{MM})\} d\underline{r}_{QM} d\underline{r}_{MM}, \quad \beta = \frac{1}{k_B T} \quad (20)$$

Here, k_B and T are respectively the Boltzmann constant and the absolute temperature. The integration is over all QM and MM degrees of freedom. The total free energy of the system is

$$A_T = -\frac{1}{\beta} \ln(Z_T) = -\frac{1}{\beta} \ln \left[\int \exp\{-\beta E_T(\underline{r}_{QM}, \underline{r}_{MM})\} d\underline{r}_{QM} d\underline{r}_{MM} \right] \quad (21)$$

By focusing on a selected subset of the system (i.e., the QM subsystem), we can define the PMF of the QM/MM system in terms of the QM atom conformation.

$$\begin{aligned} Z(\underline{r}_{QM}) &= \int \exp\{-\beta E_T(\underline{r}_{QM}, \underline{r}_{MM})\} d\underline{r}_{MM} \\ A(\underline{r}_{QM}) &= -\frac{1}{\beta} \ln\{Z(\underline{r}_{QM})\} \\ &= -\frac{1}{\beta} \ln \left[\int \exp\{-\beta E_T(\underline{r}_{QM}, \underline{r}_{MM})\} d\underline{r}_{MM} \right] \end{aligned} \quad (22)$$

Integration of this PMF in the $\{\underline{r}_{QM}\}$ space recovers the total free energy of the system.

$$A_T = -\frac{1}{\beta} \ln \left[\int \exp\{-\beta A(\underline{r}_{QM})\} d\underline{r}_{QM} \right] \quad (23)$$

Equation 22 is of great utility since the configuration space of the whole reaction system is now expressed as PMF of the QM subsystem. This reduction in dimensionality of the size of QM problem is similar to the one observed in implicit solvation

models. Assuming ergodicity in MD sampling, this PMF surface fully accounts for the thermodynamic contributions of the MM subsystem.³⁷ Dynamic contributions of the QM subsystem may be approximated by computing vibrational frequencies of the QM subsystem. For most heterogeneously catalyzed reactions, especially if water is not part of the reaction coordinate, periodic planewave calculations should be sufficient for this purpose.

To avoid convergence problems associated with MM sampling and to improve the computational efficiency, we perform a geometry optimization of the QM subsystem on this PMF in a fixed ensemble of MM conformations. This procedure permits evaluation of PMF and its gradient defined within this fixed ensemble. The free energy difference between two QM conformations α and β is calculated using the free energy perturbation expression.

$$\Delta A_{\alpha \rightarrow \beta} = -\frac{1}{\beta} \ln \langle \exp\{-\beta [E_T(\underline{r}_{QM(\beta)}, \underline{r}_{MM})] - E_T(\underline{r}_{QM(\alpha)}, \underline{r}_{MM})] \} \rangle_{\alpha, \{\underline{r}_{MM}\}} \quad (24)$$

Subscript α indicates that MM sampling is performed using the initial QM conformation and subscript $\{\underline{r}_{MM}\}$ indicates the use of a fixed ensemble of MM conformations. Using approximate total energy functions we obtain

$$\begin{aligned} \Delta A_{\alpha \rightarrow \beta} &= -\frac{1}{\beta} \ln \left[\frac{1}{N} \sum_{\tau=1}^N \exp\{-\beta \Delta \tilde{E}_T(\tau)\} \right] \\ \Delta \tilde{E}_T(\tau) &= [\tilde{E}_T(\underline{r}_{QM(\beta)}, \underline{r}_{MM}(\tau)) \\ &\quad - \tilde{E}_T(\underline{r}_{QM(\alpha)}, \underline{r}_{MM}(\tau))]_{\alpha}, \quad \tau \in \{\underline{r}_{MM}\} \end{aligned} \quad (25)$$

Considering α as reference conformation of the QM subsystem and β as conformation of the QM subsystem at current optimization step, the gradient of eq 25 with respect to the k -th QM coordinate is

$$\frac{\partial A(\underline{r}_{QM})}{\partial \underline{r}_{QM,k}} = -\frac{1}{\beta} \frac{\partial}{\partial \underline{r}_{QM,k}} \ln \left[\frac{1}{N} \sum_{\tau=1}^N \exp\{-\beta \Delta \tilde{E}_T(\tau)\} \right] \quad (26)$$

$$\begin{aligned} \frac{\partial A(\underline{r}_{QM})}{\partial \underline{r}_{QM,k}} &= \frac{\sum_{\tau=1}^N \left[\exp\{-\beta \Delta \tilde{E}_T(\tau)\} \frac{\partial \tilde{E}_T(\underline{r}_{QM}, \underline{r}_{MM}(\tau))}{\partial \underline{r}_{QM,k}} \right]}{\sum_{\tau=1}^N \exp\{-\beta \Delta \tilde{E}_T(\tau)\}} \\ &= \left\langle \frac{\partial \tilde{E}_T(\underline{r}_{QM}, \underline{r}_{MM}(\tau))}{\partial \underline{r}_{QM,k}} \right\rangle_{\Delta \tilde{E}_T(\tau)} \end{aligned} \quad (27)$$

In other words, the gradient of the PMF is simply an ensemble average of the gradients of the QM atoms and may be evaluated from the same fixed-size ensemble of MM conformations. Substituting eq 19 in eq 27, the complete expression for gradients becomes

$$\begin{aligned} \frac{\partial A(\underline{r}_{QM})}{\partial \underline{r}_{QM,k}} &= \frac{\partial \langle \psi | H_{eff}(\underline{r}_{QM}, \underline{r}_{MM}^0) | \psi \rangle}{\partial \underline{r}_{QM,k}} \\ &+ \frac{\partial [E_{MM+QM/MM}^{elec+vdW}(\underline{r}_{QM}, \underline{r}_{MM}^0)]_{Q_i=0, i \in QM}}{\partial \underline{r}_{QM,k}} \\ &+ \left\langle \frac{\partial E_{QM+MM+QM/MM}^{elec(ESP)+vdW}(\underline{r}_{QM}, \underline{r}_{MM}(\tau))}{\partial \underline{r}_{QM,k}} \right\rangle_{\Delta \tilde{E}_T(\tau)} \\ &- \frac{\partial E_{QM+MM+QM/MM}^{elec(ESP)+vdW}(\underline{r}_{QM}, \underline{r}_{MM}^0)}{\partial \underline{r}_{QM,k}} \end{aligned} \quad (28)$$

Considering that the free energy is a state function and is therefore path independent, the total free energy change between two end states can be determined by introducing a sufficient number of intermediate states. Equation 24 is separately applied for each step and all such contributions are summed up. Even if the structures of such interpolated states are nonphysical, the free energy difference between the two end states will be correct. The only requirement is that the water ensembles are large enough.

2.4. Integration with eSMS. Currently, the challenge still remains on how to practically compute the SCF energy of a large “periodic” system immersed in a liquid phase environment. The principle idea of eSMS introduced here is based on our recent successes with iSMS. The key idea of iSMS has been to include the long-range metal interactions through periodic-slab calculations within the framework of DFT calculations in the absence of a solvent and to consider the effect of solvent molecules as a localized perturbation (small or large) of free-energy differences that can be described by a cluster model embedded in an implicit solvent. Specifically, we defined the free energy function for an adsorbed reactant on a “periodic” metal slab in solvent, $A_{surface+adsorbate}^{\text{liquid}}$, using a simple subtraction scheme

$$\begin{aligned} A_{surface+adsorbate}^{\text{liquid}} &= E_{surface+adsorbate}^{\text{vacuum}} - E_{cluster+adsorbate}^{\text{vacuum}} \\ &+ A_{cluster+adsorbate}^{\text{liquid}} \end{aligned} \quad (29)$$

where $E_{surface+adsorbate}^{\text{vacuum}}$ is the planewave DFT energy of the periodic slab in vacuum, $A_{cluster+adsorbate}^{\text{liquid}}$ is the free energy in solvent of a metal cluster constructed by removing selected metal atoms from the periodic-slab model and removing the periodic boundary conditions (computed using an implicit solvation model), and $E_{cluster+adsorbate}^{\text{vacuum}}$ is the DFT energy of the same cluster in vacuum. We note that eq 29 becomes exact for an infinitely large cluster. Importantly, we found that since electrons move freely in metals, they screen electric fields very well such that converged results can be obtained for very small cluster sizes of predictable shape. In eSMS we use a similar subtraction scheme to iSMS; however, we compute $A_{cluster+adsorbate}^{\text{liquid}}$ using an explicit description of the water molecules and we do not remove any metal atoms but use a QM/MM description for the computation of $A_{cluster+adsorbate}^{\text{liquid}}$ and $E_{cluster+adsorbate}^{\text{vacuum}}$. As a result, the long-range electrostatic interaction of thousands of water molecules with adsorbed reactants and transition states can be accounted for. Also, the indirect effect of water molecules on energy differences of processes on a metal surface by changing the electron density of surface metal atoms is considered as long as this interaction is short ranged; that is, it can be described with an electrostatically

embedded metal cluster approach. Considering that water molecules are included only in the $A_{cluster+adsorbate}^{\text{liquid}}$ term, only the SCF energy and gradient terms in eq 19 and eq 28 need to be replaced using eq 29. That is, total QM/MM energy function and its gradient in QM/MM-FEP-eSMS formulation are given by

$$\begin{aligned} \tilde{E}_T(\underline{r}_{QM}, \underline{r}_{MM}) &= E_{QM}^{\text{surface}}(\underline{r}_{QM}) - E_{QM}^{\text{cluster}}(\underline{r}_{QM}) \\ &+ \langle \Psi | H_{eff}(\underline{r}_{QM}, \underline{r}_{MM}^0) | \Psi \rangle \\ &+ [E_{MM+QM/MM}^{elec+vdW}(\underline{r}_{QM}, \underline{r}_{MM}^0)]_{Q_i=0, i \in QM} \\ &+ E_{QM+MM+QM/MM}^{elec(ESP)+vdW}(\underline{r}_{QM}, \underline{r}_{MM}) - E_{QM+MM+QM/MM}^{elec(ESP)+vdW}(\underline{r}_{QM}, \underline{r}_{MM}^0) \end{aligned} \quad (30)$$

$$\begin{aligned} \frac{\partial A(\underline{r}_{QM})}{\partial \underline{r}_{QM,k}} &= \frac{\partial E_{QM}^{\text{surface}}(\underline{r}_{QM})}{\partial \underline{r}_{QM,k}} - \frac{\partial E_{QM}^{\text{cluster}}(\underline{r}_{QM})}{\partial \underline{r}_{QM,k}} \\ &+ \frac{\partial \langle \psi | H_{eff}(\underline{r}_{QM}, \underline{r}_{MM}^0) | \psi \rangle}{\partial \underline{r}_{QM,k}} \\ &+ \frac{\partial [E_{MM+QM/MM}^{elec+vdW}(\underline{r}_{QM}, \underline{r}_{MM}^0)]_{Q_i=0, i \in QM}}{\partial \underline{r}_{QM,k}} \\ &+ \left\langle \frac{\partial E_{QM+MM+QM/MM}^{elec(ESP)+vdW}(\underline{r}_{QM}, \underline{r}_{MM}(\tau))}{\partial \underline{r}_{QM,k}} \right\rangle_{\Delta \tilde{E}_T(\tau)} \\ &- \frac{\partial E_{QM+MM+QM/MM}^{elec(ESP)+vdW}(\underline{r}_{QM}, \underline{r}_{MM}^0)}{\partial \underline{r}_{QM,k}} \end{aligned} \quad (31)$$

The first two terms in eq 30 correspond to the first two terms in eq 29 and are evaluated for a periodic slab in vacuum and a QM cluster in vacuum, respectively. All other terms in eq 30 are included following eq 19, and collectively account for QM cluster in explicit solvent. Equation 31 is similarly obtained by combining eq 28 and eq 29.

Next, we list a step-by-step procedure for performing geometry optimizations using eSMS. The sequential MD-sampling, QM-optimization algorithm is similar to the one developed by Hu et al.³⁸

- (1) Set optimization cycle $n = 0$. Optimize the adsorbate on a periodic metal slab using planewave QM calculations.
- (2) Expand the model and add water molecules.
- (3) Equilibrate the water using MD simulation, keeping all metal and adsorbate atoms fixed at $\{\underline{r}_{QM}^{(0)}\}$ without any charges assigned to them. Save the last water conformation.
- (4) Select an appropriate QM cluster-in-water model containing all adsorbate atoms and only “active” metal atoms. Remaining metal atoms in the expanded periodic box and all water molecules constitute the MM subsystem.
- (5) Remove all MM water molecules and MM metal atoms from step (4) to obtain QM cluster-in-vacuum model.
- (6) Determine the lowest energy-spin state for QM cluster-in-vacuum model from step 5.
- (7) Set optimization cycle $n = n + 1$. Evaluate charges of QM atoms in the electrostatic potential of reference MM conformation.

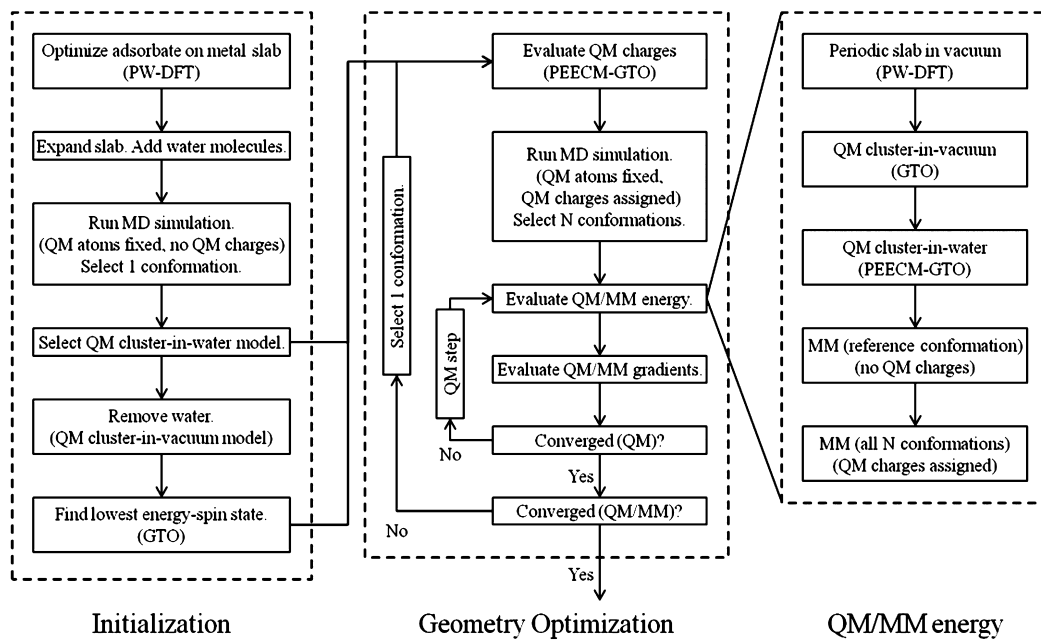


Figure 1. Algorithm for geometry optimization using eSMS method. Abbreviations used for QM methods are PW (planewave), GTO (Gaussian-type orbitals), PEECM (periodic electrostatic embedded cluster method).

- (8) Using QM charges obtained in step 7 and keeping the QM atoms fixed at $\{r_{QM}^{(n-1)}\}$, equilibrate the system using MD simulations and sample a set of MM conformations, $\{r_{MM}^{(n)}(\tau), \tau = 1 \dots N\}$, where N is the number of MM conformations sampled.
- (9) With the MM ensemble fixed at $\{r_{MM}^{(n)}(\tau)\}$, minimize the PMF of the QM subsystem as given by eq 30. The corresponding gradient is given by eq 31. For each evaluation of QM energy or gradient, we need
 - (a) planewave QM calculation for periodic slab in vacuum (first term on RHS of eq 30),
 - (b) QM calculation for cluster-in-vacuum model using Gaussian-type orbitals (second term on RHS of eq 30),
 - (c) QM calculation and evaluation of QM charges for cluster-in-water model using Gaussian-type orbitals and a periodic electrostatic embedding scheme (third term on RHS of eq 30),
 - (d) MM calculation for reference MM conformation without any charges assigned to QM atoms (fourth term on RHS of eq 30), and
 - (e) MM calculation for each sampled conformation in $\{r_{MM}^{(n)}(\tau)\}$ where the QM atoms are assigned charges as determined in step c (5–sixth terms on RHS of eq 30).
 - (f) Steps a–d can be performed simultaneously or sequentially in any order, but must precede step e. The MM calculations in step e are independent of each other and may be performed in any arrangement, considering efficient utilization of computational resources. Coordinates of the QM atoms must remain synchronized among all QM and MM models.
- (10) Go to step 7 until converged.

The main feature of this iterative algorithm (Figure 1) is the use of a finite, fixed-size ensemble of MM conformations for each QM optimization sequence. The PMF of QM coordinates

and its gradient can be evaluated precisely within this ensemble, circumventing statistical convergence problems with MD sampling. The starting QM structure is already optimized in vacuum and should serve as an excellent initial guess for most cases. During iterative sampling/optimization cycles, each optimized QM structure serves as the reference QM structure for next cycle, and improves the one from the previous step by providing better QM charges and total QM/MM energy. Convergence is generally obtained within a few cycles.

3. COMPUTATIONAL DETAILS

3.1. Periodic Planewave QM Calculations. Periodic DFT calculations were performed using the Vienna Ab Initio Simulation Package (VASP 5.2).^{40,41} A planewave basis set with a cutoff energy of 400 eV and an SCF convergence criterion of 1.0×10^{-7} eV were employed for the valence electrons. Ionic core potentials were described using the projector augmented wave (PAW) method.⁴² Electron exchange and correlation effects were accounted for using the Perdew–Burke–Ernzerhof (PBE) density functional^{43,44} within the generalized gradient approximation (GGA). The Pt (111) surface was simulated using a large 4×4 unit cell with four layers of metal atoms and a vacuum of 15 Å to minimize interaction between periodically repeated images. A $4 \times 4 \times 1$ Monkhorst–Pack k-point grid⁴⁵ was employed for sampling the Brillouin zone. Dipole and quadrupole corrections to the energy were included using the modified Makov–Payne method.⁴⁶ Harris–Foulkes-type corrections for forces were included. Fractional occupancies of bands were allowed within a window of 0.10 eV using the first-order Methfessel–Paxton smearing method.⁴⁷ The bottom two Pt layers were fixed in their bulk positions. All structures were optimized to a force smaller than 0.02 eV/Å on each relaxed atom. Γ -point only, single-point energy calculations were performed for expanded surfaces and for periodic cluster models. Spin-polarization effects were taken into account for periodic cluster models. A combination of climbing-image nudged elastic band^{48,49} and dimer^{50,51} methods was used for

the transition state search. All minima and transition state structures were confirmed through dynamical matrix calculations. For iSMS and eSMS calculations, the SCF energy convergence criterion was set to 1.0×10^{-8} eV.

3.2. Nonperiodic QM Calculations. Cluster-model calculations without periodic boundaries were performed using the TURBOMOLE 6.4 program package.^{52–55} Adsorbate atoms including water molecules were represented using all-electron basis sets of triple- ζ quality.^{56,57} Pt atoms were represented using relativistic small-core effective core potentials (ECPs) together with a triple- ζ quality basis set for the valence electrons.^{58,59} Electron exchange and correlation effects were accounted for using the PBE functional. The RI-J approximation with auxiliary basis sets was used to approximate Coulomb potentials.^{60,61} For each QM cluster model, multiple spin states were tested using an SCF energy convergence criterion of 1.0×10^{-7} Hartree and spherical grid m4.⁵⁸ For iSMS and eSMS calculations, the SCF energy convergence criterion and spherical grid were changed to 1.0×10^{-8} Hartree and m5, respectively. These calculations were performed only for the lowest-energy spin state.

3.3. Implicit Solvation (iSMS). For implicit solvation, COSMO^{14,62,63} and COSMO-RS^{64–66} calculations were performed using radii-based cavities and a dielectric constant of infinity. The structures were first optimized in the iSMS calculations with all metal atoms fixed until the maximum force on each relaxed atom was smaller than 1.0×10^{-3} au. Only for optimized geometries, COSMO-RS calculations were performed using the COSMOtherm program.⁶⁶ Thermodynamic properties of water (solvent) were obtained from the COSMOtherm database, based on parametrization of the results of quantum chemical COSMO calculations at the BP-TZVP level of theory. COSMO-RS input files for iSMS-optimized structures were generated from single-point COSMO calculations using B-P86 functional^{67,68} and TZVP basis set. All other settings are the same as described in section 3.2.

3.4. Explicit Solvation (eSMS). QM calculations in a field of MM water molecules were performed using the periodic electrostatic embedded cluster method (PEECM)⁶⁹ with point charges taken from the TIP3P water model.⁷⁰ The periodic box used for these calculations is described in section 3.5. Charges on QM atoms were estimated using natural population analysis (NPA).⁷¹ ESP-fitted charges were initially used. However, considering their high computational cost,⁷² NPA charges were adopted. Approximations made in eq 8 and 9 were tested against QM calculations. These results are presented in section 4.3. All other settings are same as described in section 3.2.

3.5. Molecular Dynamics Simulations. MD simulations were performed using the DL_POLY 4.03 molecular simulation package.⁷³ The original 4×4 Pt (111) unit cell was expanded to a 16×20 lateral surface and more vacuum was added in Z-direction. The final box ($45.0 \text{ \AA} \times 48.7 \text{ \AA} \times 50.0 \text{ \AA}$) contained 1280 Pt atoms. Any additional adsorbates created by this expansion were deleted. The simulation box was filled with 2250 water molecules to obtain a liquid density of 0.83 g/cm^3 , approximately the density of saturated liquid water at 500 K. All Pt and adsorbate atoms were kept fixed, whereas the water molecules were constrained to TIP3P geometry using the SHAKE algorithm.⁷⁴ Simulations were performed in a canonical (NVT) ensemble with Berendsen thermostat⁷⁵ using a relaxation constant of 0.01 ps. Smoothed Particle Mesh Ewald (SPME) method⁷⁶ with a cutoff of 10 Å was employed for

electrostatic interactions. The same cutoff was used for van der Waals interactions. A time step of 1 fs was used. The system was first equilibrated for 100 ps. Then, an ensemble of 10 000 MM conformations was generated by recording every 10th conformation from an additional 100 ps of simulation.

Force field parameters for water were taken from the TIP3P model. For the Pt–water interaction, the Spohr–Heinzinger potential⁷⁷ was implemented in the DL_POLY source code. Only van der Waals' parameters for adsorbate (ethylene glycol) atoms were taken from the OPLS force field,^{78,79} whereas charges for these atoms were obtained from the QM calculations as described in section 3.4. For Pt atoms that are included in the QM cluster, NPA charges obtained from QM calculations were used; other Pt atoms were not assigned any charge. We note that there is hardly any charge transfer between liquid water and the metal surface and the computed charges on the metal atoms are very small.⁷² As a result, the Spohr–Heinzinger potential does in effect not contain any electrostatic interaction such that the electrostatic interaction computed by NPA charges on the metal atoms does not lead to overcounting of any interactions. We nevertheless had to include the NPA charges on the metal atoms to ensure overall charge neutrality of our reaction system. Lorentz–Berthelot mixing rules are used for Lennard–Jones interaction parameters between adsorbed ethylene glycol species and the TIP3P water molecules.

3.6. Implementation of iSMS and eSMS. The algorithm listed in section 2.4 has been implemented using a set of FORTRAN programs. Of particular importance are programs that calculate the SCF energy and gradients for a given structure using the iSMS and eSMS methods. These programs replace standard SCF energy and gradient routines and may be called from any external optimizer without knowledge of implementation details. A modular approach has been adopted in program design such that a new QM or MM package can be integrated by simply including respective input/output file parsing routines. Using predefined templates and a set of keywords for the specific task, input files for all QM and MM programs are automatically generated. The job resource manager then executes the respective binaries in the order described in section 2.4. Synchronization of QM coordinates among all programs is guaranteed at all times. When calculations are finished, all output files are automatically processed to extract required information.

4. RESULTS AND DISCUSSION

C–C cleavage in double-dehydrogenated ethylene glycol, with one H atom removed from each C atom, has been used as a model reaction for this study.



The choice of this reaction has been influenced by a number of factors. First, the focus of this study is to develop and validate a theoretical method to account for solvent effects on elementary processes occurring at metal surfaces relevant for liquid phase processing of lignocellulosic biomass model molecules. Although the eSMS formulation allows water molecules to be treated as part of the reaction coordinate, such a system is beyond the scope of this study. Second, FEP calculations with finite configuration space sampling require significant overlap in importance of initial and final state configurations. This can be achieved by splitting the reaction coordinate into a number of small FEP windows. A very high activation barrier or a

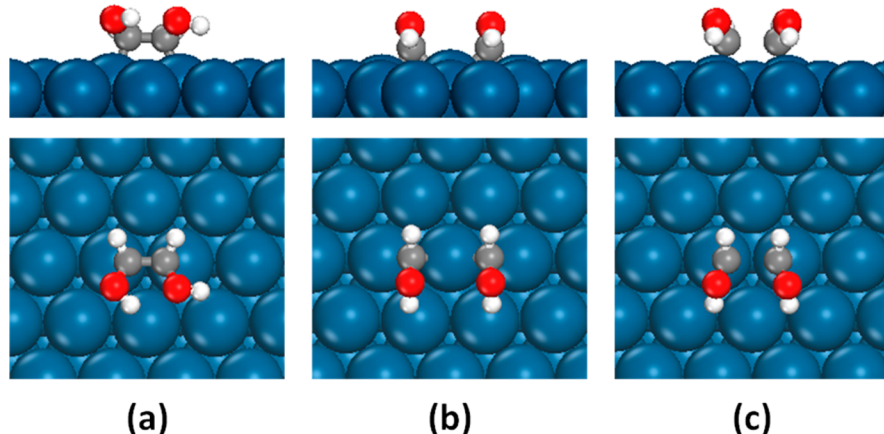


Figure 2. Side (upper panel) and top (lower panel) views of optimized structures on Pt (111) slab in vacuum: (a) reactant, (b) coadsorbed products, and (c) transition state for the reaction $\text{CHOH}-\text{CHOH} \rightarrow 2(\text{CHOH})$.

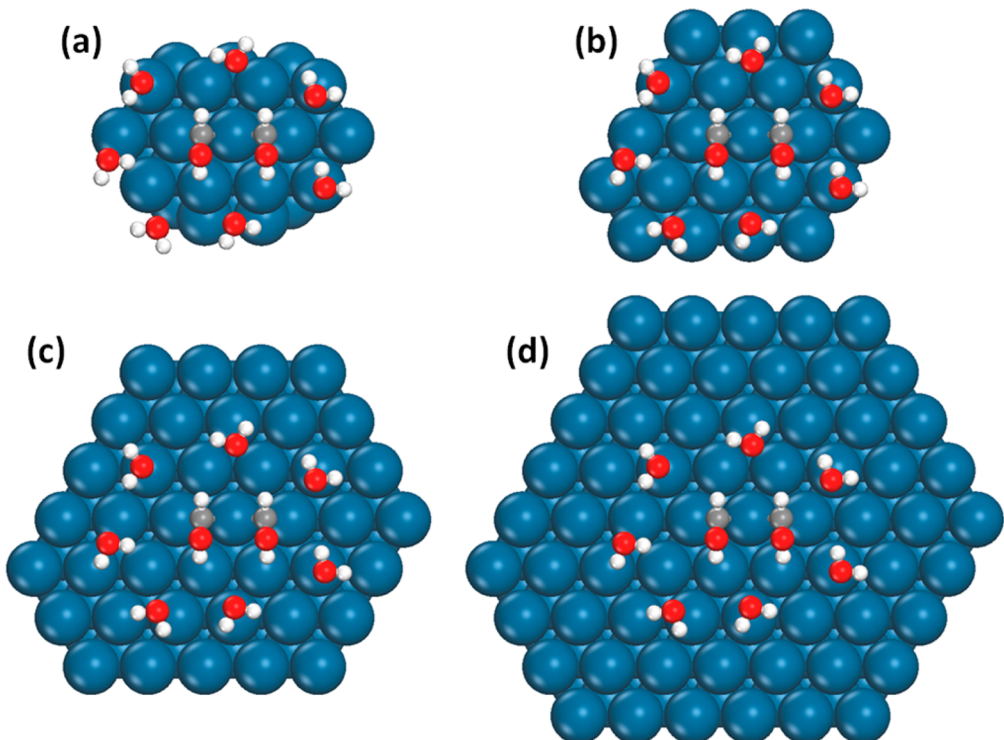


Figure 3. QM clusters selected for convergence test of eSMS with respect to cluster size: final state with 7 water molecules is shown. (a) Cluster contains Pt atoms directly bound to CHO_H species and their nearest neighbors. (b) Cluster contains all Pt atoms of cluster a plus additional rows of Pt atoms involved in screening the Pt atoms that form chemical bounds to CHO_H species. (c) Cluster contains all Pt atoms of cluster b plus an additional ring of Pt atoms. (d) Benchmark cluster model.

geometrically complex reaction coordinate would become computationally prohibitive. At the same time, if the activation barrier is too low, the PMF procedure might not be valid and it would be difficult to characterize the effect of water. Partial dehydrogenation of both C atoms ensures that all structures involved in the selected reaction coordinate bind to the Pt (111) surface sufficiently strongly resulting in a moderately high activation barrier. We avoided complete dehydrogenation which would result in a very small activation barrier. Finally, the initial state contains two OH groups on adjacent C atoms, a characteristic feature of biomass-derived polyols, and thus serves well our long-term goal of modeling aqueous-phase processing of such molecules.

4.1. Convergence of eSMS. For practical applications, the SMS energy function must converge for clusters of small size and predictable shape. For the iSMS method, we have previously shown that a two-layer QM cluster including metal atoms forming the adsorption site and their nearest neighbors should be sufficient.¹⁷ The results of a similar convergence test with explicit QM water molecules are presented here.

In its most stable configuration, CHOH-CHOH is adsorbed on a bridge site with each C atom binding to one Pt atom. A hydrogen bond is formed between the two OH groups (Figure 2a). C-C cleavage results in formation of two CHOH fragments that are coadsorbed on the same slab. Multiple coadsorption sites were tested and the lowest-energy combination was found to involve two adjacent bridge sites

(Figure 2b). In all cases, C atoms satisfy their tetrahedral bonding geometries.

For explicit solvation, seven water molecules of TIP3P geometry were “randomly” placed around the adsorbates. To avoid large changes in water–water and water–metal interaction, the same configuration of water molecules was used for both the initial and final states. The original 4×4 unit cell was expanded to a 12×12 unit cell and any additional adsorbates and water molecules created by this expansion were removed. For this convergence test, it is necessary to disrupt the formation of a continuous hydrogen bonding network that cannot be reproduced in nonperiodic QM calculations described in section 3.2. Planewave calculations estimate $\Delta E_{\text{surface},\text{rxn}}^{\text{water}} = 0.23$ eV and $\Delta E_{\text{surface},\text{rxn}}^{\text{vacuum}} = 0.14$ eV. That is, the reaction becomes endothermic by 0.09 eV in the presence of water. These values are used as reference for analyzing the performance of the eSMS method for various QM clusters.

Next, QM clusters were carved out from the expanded slabs. We have considered 4 types of clusters in terms of size of their lateral surface area (Figure 3). For each type, 1–4 layers of Pt atoms were considered. Figure 4 confirms the smooth and rapid

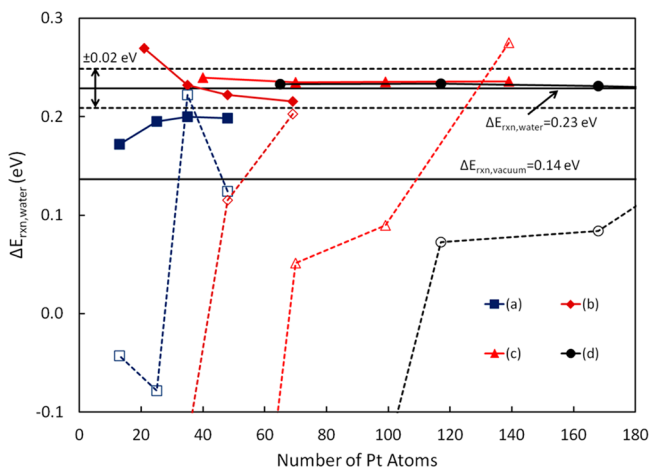


Figure 4. Convergence of eSMS with size of QM cluster (computed with VASP 5.2). Solid horizontal lines show reference values for $\Delta E_{\text{surface},\text{rxn}}^{\text{water}}$ and $\Delta E_{\text{surface},\text{rxn}}^{\text{vacuum}}$ for a $12 \times 12 \times 4$ Pt (111) slab. Dashed horizontal lines mark a tolerance of ± 0.02 eV about $\Delta E_{\text{surface},\text{rxn}}^{\text{water}}$. Solid lines with filled markers are eSMS results for the 4 types of QM clusters shown in Figure 3. Dashed lines with hollow markers are corresponding results for $\Delta E_{\text{cluster},\text{rxn}}^{\text{water}}$ without using eSMS. For each cluster type, 1–4 layer thick clusters are considered. 233-atom, 4-layer cluster of type d is not shown on this scale.

convergence of eSMS as a function of lateral size and depth of the QM clusters. Clusters of type a clearly fail to include some Pt atoms that are in direct vicinity to the adsorbate. These clusters are not useful regardless of their thickness. Two- and three-layer clusters of type b contain the same number of atoms as 3- and 4-layer clusters of type a, respectively. However, because all Pt atoms in close proximity to the adsorbate are now included, these clusters are able to meet a tolerance of ± 0.02 eV. All clusters of types c and d produce excellent agreement with the reference calculation.

Figure 4 also emphasizes the importance of long-range metal interactions. When eSMS is not used, even the largest clusters fail to match the results of the periodic slab calculations and there is no smooth convergence pattern. This behavior is expected because it just illustrates the reasons why periodic

models are commonly used for metallic systems. On the other hand, when these interactions are included using eSMS, all four types of clusters show smooth convergence with increasing size clearly illustrating that the indirect effect of water molecules on energy differences of processes on a metal surface by changing the electron density of surface metal atoms is short ranged as required for eSMS.

4.2. Integration of Periodic and Nonperiodic QM Calculations. To test the integration of periodic (planewave basis) and nonperiodic (Gaussian-type basis) QM calculations, TURBOMOLE calculations have been performed for selected two-layer clusters with and without water molecules. All water molecules are assigned the same basis sets as other adsorbate atoms in the system. Figure 5 shows that, when using the eSMS

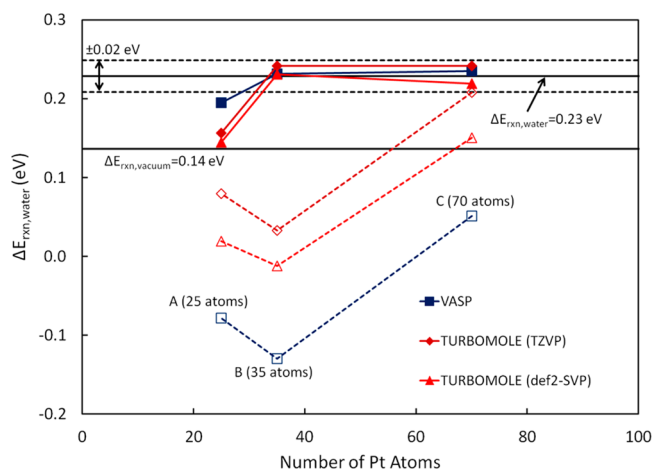


Figure 5. Convergence of eSMS with size of QM cluster (periodic planewave QM calculations integrated with nonperiodic QM calculations). Solid horizontal lines show reference values of $\Delta E_{\text{surface},\text{rxn}}^{\text{water}}$ and $\Delta E_{\text{surface},\text{rxn}}^{\text{vacuum}}$ for a $12 \times 12 \times 4$ Pt (111) slab. Dashed horizontal lines mark a tolerance of ± 0.02 eV around $\Delta E_{\text{surface},\text{rxn}}^{\text{water}}$. Solid lines with filled markers are eSMS results for two-layer clusters of types a, b, and c, as shown in Figure 3. Dashed lines with hollow markers are corresponding results for $\Delta E_{\text{cluster},\text{rxn}}^{\text{water}}$.

method, results obtained from our integrated calculations are in good agreement with pure planewave calculations. We again see that the smallest cluster that is able to satisfy the specified tolerance in all cases is a 35-atom, two-layer cluster of type b. It agrees with all our previous conclusions, because (1) all metal atoms directly involved in bonding and their nearest neighbors are included and (2) there are at least 2 layers of Pt atoms. These conclusions hold even when a smaller basis set is used. We have previously shown that the iSMS method also converges for small basis sets.¹⁷

4.3. Validation of Approximate Total QM/MM Energy Function. In order to test the effectiveness of fixed-charge approximation made in eq 8, we have compared the results obtained from eq 19 against ab initio QM calculations. As a test case, we have considered the initial state (CHOH–CHOH) adsorbed on a two-layer, 51-atom cluster (Figure 6). The simulation box contains a total of 1280 Pt atoms and 2250 TIP3P water molecules. This QM cluster is an intermediate between the 35- and 70-atom clusters (Figure 5). Although we have already demonstrated the usefulness of the 35-atom cluster for this particular reaction, considering that our long-term goal is modeling the aqueous phase reforming mechanism of ethylene glycol and glycerol, and noting that the 35-atom

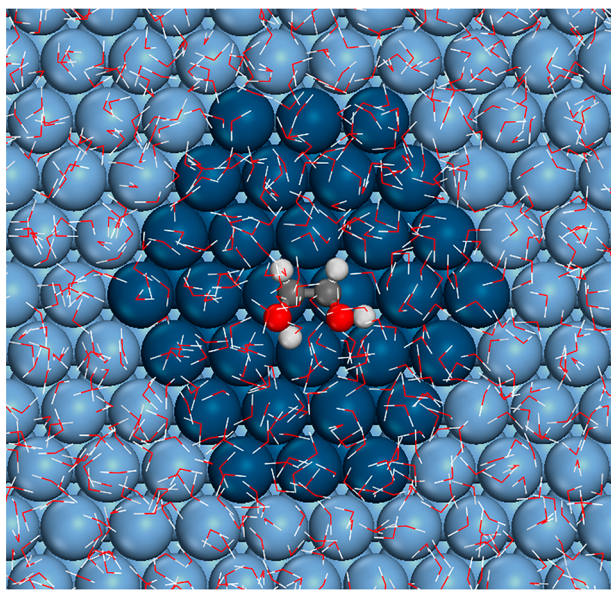


Figure 6. Initial state of dehydrogenated ethylene glycol on a two-layer, 51-atom cluster with 2250 TIP3P water molecules. Pt-QM (dark blue), Pt-MM (light blue), C-QM (gray), O-QM (red), and H-QM (white) atoms are shown as solid spheres. MM water molecules are shown as lines with O (red) and H (white) vertices.

cluster may not be sufficient for some of the larger multidentate intermediates in these mechanisms, a larger 51-atom cluster was chosen for all further studies. This particular QM cluster satisfies all previously listed requirements for all elementary reactions in these mechanisms.

After filling the simulation box with water molecules, the system was equilibrated for 100 ps. The objective is to obtain a reasonable water conformation that can be used for evaluation of NPA charges on the QM atoms. Using the last water conformation from this simulation, periodic electrostatic embedded cluster method (PEECM)⁶⁹ calculations were performed and NPA (natural population analysis)⁷¹ charges for the QM atoms were determined. These charges were updated in the MM force field, and the system was again equilibrated for 100 ps. From the next 100 ps of MD simulation, 50 water conformations, 2 ps apart, were recorded.

For each of these 50 conformations, the QM energy was obtained from PEECM calculations. In other words, each sampled conformation was treated as a reference MM conformation. Equation 19 for this case reduces to

$$E_T(\underline{r}_{QM}, \underline{r}_{MM}^0) = \langle \Psi | H_{eff}(\underline{r}_{QM}, \underline{r}_{MM}^0) | \Psi \rangle + [E_{MM+QM/MM}^{elec+vdW}(\underline{r}_{QM}, \underline{r}_{MM}^0)]_{Q_i=0, i \in QM} \quad (33)$$

Only those electrostatic and van der Waals interactions need to be included in the MM force field that are not accounted for by the PEECM calculations. No NPA fitted charges are required for the QM atoms. We then perturbed the QM atom geometry characteristic of an FEP step and recalculated the QM energies for the same fixed ensemble of 50 conformations.

Total QM/MM energies for both initial and perturbed QM geometries were also estimated by application of eq 19, that is, making the fixed-charge approximation. That is, PEECM calculations were performed only for one water conformation and the QM energy and NPA charges obtained from this

calculation were used to approximate \tilde{E}_T for all other conformations. Figure 7 shows that the energy differences

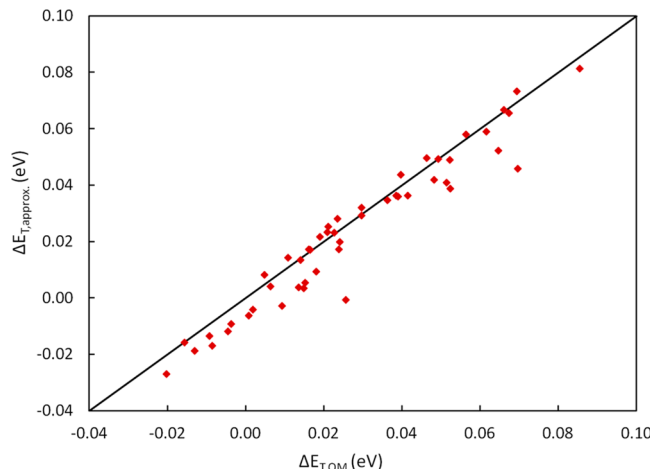


Figure 7. Validation of fixed-charge approximation. Difference between total QM/MM energies of 2 QM conformations is evaluated in an ensemble of 50 representative water conformations using exact QM calculations (X-axis) and with the assumption of fixed QM charges (Y-axis).

obtained using the fixed-charge approximation are in good agreement with those obtained from ab initio calculations. If the free energy difference is estimated from these data sets using the FEP procedure, the error is smaller than 5 meV (6%).

4.4. Optimization of Reactant, Product, and Transition States. Optimizations of reactant, product, and transition states were performed using the QM/MM-FEP algorithm described in section 2.4. Structures obtained from planewave calculations on the Pt (111) slab were used as starting points. Each optimization cycle started with a 200 ps MD simulation which includes 100 ps of equilibration. An ensemble of 10 000 MM water conformations was recorded in this step. The structures were then optimized in this fixed ensemble with all metal atoms fixed until the maximum force on each relaxed atom was smaller than 1.0×10^{-3} au. QM atom conformations and NPA charges thus obtained were used in the next cycle of MD sampling and QM atom optimization. All optimizations were carried out using the def2-SVP basis set and PBE functional.

Convergence of relative free energies over a number of optimization cycles is shown in Figure 8. There is a negligible effect of water on the transition state. The products state is stabilized in water by 1.8 kJ/mol. The reactant state is most affected by the presence of water as it is stabilized by 9.3 kJ/mol. Structural changes observed during these optimizations are summarized in Table 1. These changes, however small, are consistent in all cases: C–Pt bond is shortened whereas C–O, C–H, and O–H bonds are elongated. Changes observed for C–O and O–H bonds are noticeably larger than for C–H bonds. The most significant effect of water is observed for the intramolecular hydrogen bond in the reactant state that is elongated by 0.24 Å. This change is caused by rotation of one OH group (H of hydrogen bond) away from the other OH group toward the surface, in a direction similar to the transition and product states. The torsional angle between the two OH groups is changed by 28°.

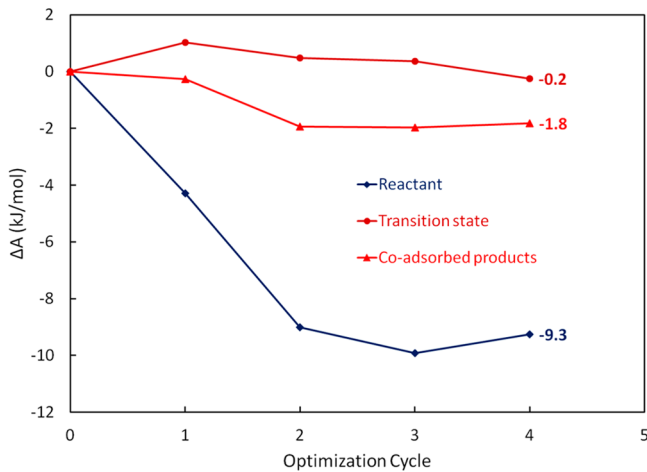


Figure 8. Liquid-phase optimization of reactant, product, and transition states using QM/MM-FEP. All free energies are relative to the respective initial states.

Table 1. Structural Changes in the Presence of Water for Reactant, Product and Transition State^a

bond	reactant	product	transition state
C-Pt	-0.036	-0.037	-0.022
C-C	+0.005		+0.024
C-O	+0.016	+0.030	+0.007
C-H	+0.002	+0.001	+0.002
O-H	+0.011	+0.001	+0.004
O-H (hydrogen bond)	+0.237		

^aChanges (Å) are measured after four cycles of QM/MM-FEP optimization relative to planewave-optimized structures on a Pt (111) slab. For multiple bonds of same type, only average changes are reported.

For comparison, we also performed these optimizations using the iSMS method starting from the same initial structures. All optimizations were carried out using the def2-SVP basis set and PBE functional. Single-point energy calculations were performed for the optimized structures using TZVP basis set and B-P86 functional to generate input files for COSMO-RS. The reactant, product and transition state structures were stabilized in the presence of water by 2.4, 0.3, and 0.3 kJ/mol, respectively. All bond length changes are negligible. The torsional angle between the two OH groups is changed by only 2° and the resultant increase in the length of hydrogen bond is 0.03 Å. This inconsistency between iSMS and eSMS results is not surprising since such site-specific interactions are difficult to describe with implicit solvation models.

4.5. Free Energy Profile. With three states known on the reaction coordinate, a complete free energy profile was constructed by inserting intermediate states. To obtain a smooth potential energy surface, atomic overlaps introduced by linear interpolation were removed. For this purpose, selective geometry optimizations were performed for these intermediate states by fixing both C atoms at the interpolated coordinates. O and H atoms of the adsorbates were relaxed for 20 steps. These optimizations were not pursued to convergence. Considering that the thermal energy ($k_B T$) at 500 K is 0.043 eV, more intermediate states were introduced where necessary to ensure that no two adjacent images differ in energy by more than this value. In the end, there were 41 intermediate states between the reactant and transition state and 34 intermediate states between

the product and transition state. QM/MM-FEP calculations were performed for all such windows to obtain the complete free energy profile (Figure 9). A summary of our results that includes vibrational contributions to the free energy of the stationary points is presented in Table 2.

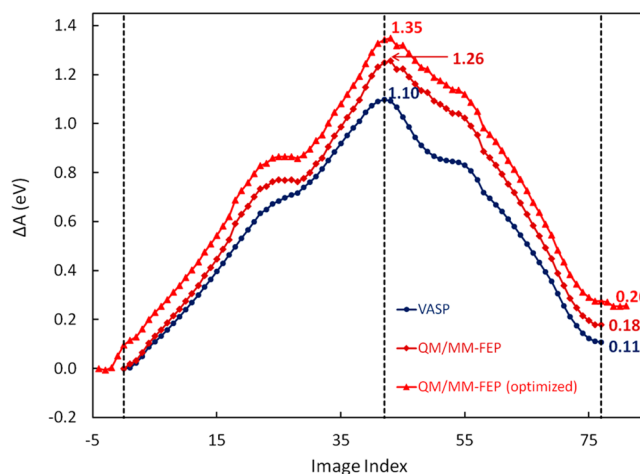


Figure 9. Free energy profile (without vibrational contributions to the partition function/free energy) for the reaction $\text{CHOH}-\text{CHOH} \rightarrow 2(\text{CHOH})$. Dashed vertical lines correspond to gas-phase structures of the reactant state (index = 0), transition state (index = 42), and product state (index = 77). For index 0 to 77 the QM/MM-FEP profile is calculated using the same structures as in the gas phase. Results of QM/MM-FEP optimization are included to the left of the gas phase reactant state (index < 0) and to the right of gas phase product state (index > 77). In addition, the gas phase transition state structure is replaced with the transition state structure obtained in liquid water and steps to the left and right are recalculated. The difference between the results depicted here and Table 2 originate from the inclusion of vibrational contributions in Table 2.

Table 2. Effect of Water on Reaction Free Energy and Activation Barrier^a

	activation barrier (eV)	reaction energy (eV)
VASP-Pt (111) slab	+1.04	+0.05
eSMS (gas-phase structures)	+1.20	+0.12
eSMS (optimized in water)	+1.25	+0.15
iSMS (gas-phase structures)	+1.13	+0.15
iSMS (optimized in water)	+1.15	+0.16

^aFor gas-phase and iSMS-optimized structures vibrational frequencies are calculated in the gas phase (as it is common for COSMO-RS calculations). For eSMS-optimized structures, vibrational frequencies are computed assuming molecular vibrations occur on a time scale that does not allow re-orientation of the solvent molecules.

For eSMS-optimized structures, frequency calculations were performed using numerical gradients and central differences with a step size of 0.02 au. These calculations assumed nonequilibrium solvation, that is, the vibrations of the QM subsystem occur at a time scale that does not allow reorientation of the surrounding water environment. For all other cases reported in Table 2, gas-phase frequencies obtained from periodic-slab calculations were used to calculate vibrational contributions to the free energy.

Results obtained from both iSMS and eSMS are in good qualitative agreement. The reaction becomes more endothermic in the presence of water by about 10 kJ/mol. The

activation barrier also increases by 10–20 kJ/mol. The effect of water in all cases can be traced back to a strong effect of water on the reactant state. Larger changes are predicted in water when using explicit solvent molecules and can be attributed to larger structural changes, especially in hydrogen bonding.

4.6. Computational Efficiency. The total MD simulation time for the free energy profile shown in Figure 9 exceeds 25 ns. This is almost 3 orders of magnitude longer than any previously reported ab initio MD simulation for metal surfaces. The total computational cost to obtain the complete FEP profile (including QM/MM-FEP optimization) is however only about 25 times that of gas-phase planewave calculations for the structures (reactant, product and transition state). This is a significant improvement since the effect of an aqueous environment is correctly captured at a computational cost that should be affordable, at least for those elementary reactions in a mechanism that are likely most affected by water.

5. CONCLUSIONS

Direct application of ab initio molecular dynamics (MD) methods for simulation of transition metal-catalyzed reactions in an aqueous environment is limited by the enormous computational cost of sampling the configuration space of such large and complex systems in a statistically relevant manner. Force field based MD simulations can adequately address the issue of configuration space sampling, but often fail to capture electronic structure changes associated with bond breaking and forming processes. Hybrid QM/MM methods offer a computationally efficient alternative and have been successfully demonstrated for numerous aqueous-phase reaction systems.

In this work, we have adopted the QM/MM-FEP method for simulation of chemical reactions at metal–water interfaces. The reaction process is modeled with our eSMS methodology that combines computations on a periodic metal slab with calculations of a finite QM metal cluster placed in a large MM water box. Long-range metal interactions are included by the periodic planewave calculations and all water effects are accounted for by the cluster model computations. Expressions for the PMF of the QM subsystem and gradient of this PMF have been derived within the QM/MM-FEP-eSMS framework. Geometry optimizations on this PMF surface are performed iteratively with sequential MD-sampling and QM atom optimization steps. A fixed-size ensemble of MM conformations is used to improve the precision of QM energy and gradient evaluations resulting in faster convergence. On-the-fly QM calculations are avoided by using the fixed-charge approximation for the QM/MM electrostatic interactions. We found this approximation to be very good for metallic systems. An overall speedup of multiple orders of magnitude is achieved compared to ab initio MD simulations.

We have demonstrated that this novel solvation scheme (eSMS) converges quickly both with size of QM cluster and basis set. Effectiveness of this new approach is illustrated by modeling the C–C bond cleavage reaction in dehydrogenated ethylene glycol at the Pt (111)/H₂O interface. Gas-phase structures of reactant, product and transition state are first optimized in water; then, the complete free energy profile for the reaction coordinate is obtained by inserting intermediate states and calculating free energy differences between adjacent states. It is shown that the reactant state is disproportionately stabilized in water, and the effect can be correlated with changes

in intramolecular hydrogen bonding. Results obtained from an implicit solvation scheme are in good agreement.

■ ASSOCIATED CONTENT

S Supporting Information

Comparison of ESP-fitted and NPA charges for a metal cluster in water is presented. This material is available free of charge via the Internet at <http://pubs.acs.org>.

■ AUTHOR INFORMATION

Corresponding Author

*Email: heyden@cec.sc.edu.

Notes

The authors declare no competing financial interest.

■ ACKNOWLEDGMENTS

This work was funded by the United States Department of Energy, Office of Basic Energy Sciences (No. DE-SC0007167). Computing resources provided by the Nanocenter at the University of South Carolina, National Energy Research Scientific Computing Center (NERSC), and Extreme Science and Engineering Discovery Environment (XSEDE) computing resources provided by the Texas Advanced Computing Center (TACC) at The University of Texas at Austin (No. TG-CTS090100) and National Institute of Computational Sciences (Nos. TG-CTS090100 and TG-DMR110037) are gratefully acknowledged.

■ REFERENCES

- (1) Rossmeisl, J.; Logadottir, A.; Norskov, J. K. Electrolysis of water on (oxidized) metal surfaces. *Chem. Phys.* **2005**, *319*, 178–184.
- (2) D'Agostino, C.; Brett, G. L.; Miedziak, P. J.; Knight, D. W.; Hutchings, G. J.; Gladden, L. F.; Mantle, M. D. Understanding the solvent effect on the catalytic oxidation of 1,4-butanediol in methanol over Au/TiO₂ catalyst: NMR diffusion and relaxation studies. *Chem.—Eur. J.* **2012**, *18*, 14426–14433.
- (3) Roudgar, A.; Eikerling, M.; van Santen, R. Ab initio study of oxygen reduction mechanism at Pt₄ cluster. *Phys. Chem. Chem. Phys.* **2010**, *12*, 614–620.
- (4) Hou, R.; Wang, T.; Lan, X. Enhanced selectivity in the hydrogenation of acetylene due to the addition of a liquid phase as a selective solvent. *Ind. Eng. Chem. Res.* **2013**, *52*, 13305–13312.
- (5) Hibbitts, D. D.; Loveless, B. T.; Neurock, M.; Iglesia, E. Mechanistic role of water on the rate and selectivity of Fischer–Tropsch synthesis on ruthenium catalysts. *Angew. Chem., Int. Ed.* **2013**, *52*, 12273–12278.
- (6) Okamoto, Y. Density-functional calculations of atomic and molecular adsorptions on 55-atom metal clusters: Comparison with (111) surfaces. *Chem. Phys. Lett.* **2005**, *405*, 79–83.
- (7) Okamoto, Y. Comparison of hydrogen atom adsorption on Pt clusters with that on Pt surfaces: A study from density-functional calculations. *Chem. Phys. Lett.* **2006**, *429*, 209–213.
- (8) Iftimie, R.; Minary, P.; Tuckerman, M. E. Ab initio molecular dynamics: Concepts, recent developments, and future trends. *Proc. Natl. Acad. Sci. U.S.A.* **2005**, *102*, 6654–6659.
- (9) Mattsson, T. R.; Paddison, S. J. Methanol at the water–platinum interface studied by ab initio molecular dynamics. *Surf. Sci.* **2003**, *544*, L697–L702.
- (10) Otani, M.; Hamada, I.; Sugino, O.; Morikawa, Y.; Okamoto, Y.; Ikeshoji, T. Structure of the water/platinum interface—A first principles simulation under bias potential. *Phys. Chem. Chem. Phys.* **2008**, *10*, 3609–3612.
- (11) Yang, J.; Dauenhauer, P. J.; Ramasubramaniam, A. The role of water in the adsorption of oxygenated aromatics on Pt and Pd. *J. Comput. Chem.* **2013**, *34*, 60–66.

- (12) Cramer, C. J.; Truhlar, D. G. Implicit solvation models: Equilibria, structure, spectra, and dynamics. *Chem. Rev.* **1999**, *99*, 2161–2200.
- (13) Tomasi, J.; Mennucci, B.; Cammi, R. Quantum mechanical continuum solvation models. *Chem. Rev.* **2005**, *105*, 2999–3093.
- (14) Klamt, A.; Schuurmann, G. COSMO: A new approach to dielectric screening in solvents with explicit expressions for the screening energy and its gradient. *J. Chem. Soc., Perkin Trans. 2* **1993**, *799*–805.
- (15) Jacob, T.; Goddard, W. A. Water formation on Pt and Pt-based alloys: A theoretical description of a catalytic reaction. *ChemPhysChem* **2006**, *7*, 992–1005.
- (16) Wang, H. F.; Liu, Z. P. Formic acid oxidation at Pt/H₂O interface from periodic DFT calculations integrated with a continuum solvation model. *J. Phys. Chem. C* **2009**, *113*, 17502–17508.
- (17) Faheem, M.; Suthirakun, S.; Heyden, A. New implicit solvation scheme for solid surfaces. *J. Phys. Chem. C* **2012**, *116*, 22458–22462.
- (18) Behtash, S.; Lu, J.; Faheem, M.; Heyden, A. Solvent effects on the hydrodeoxygenation of propanoic acid over Pd(111) model surfaces. *Green Chem.* **2014**, *16*, 605–616.
- (19) Toney, M. F.; Howard, J. N.; Richer, J.; Borges, G. L.; Gordon, J. G.; Melroy, O. R.; Wiesler, D. G.; Yee, D.; Sorensen, L. B. Voltage-dependent ordering of water molecules at an electrode–electrolyte interface. *Nature* **1994**, *368*, 444–446.
- (20) Henderson, M. A. The interaction of water with solid surfaces: Fundamental aspects revisited. *Surf. Sci. Rep.* **2002**, *46*, 1–308.
- (21) Hodgson, A.; Haq, S. Water adsorption and the wetting of metal surfaces. *Surf. Sci. Rep.* **2009**, *64*, 381–451.
- (22) Cao, D.; Lu, G. Q.; Wieckowski, A.; Wasileski, S. A.; Neurock, M. Mechanisms of methanol decomposition on platinum: A combined experimental and ab initio approach. *J. Phys. Chem. B* **2005**, *109*, 11622–11633.
- (23) Zope, B. N.; Hibbitts, D. D.; Neurock, M.; Davis, R. J. Reactivity of the gold/water interface during selective oxidation catalysis. *Science* **2010**, *330*, 74–78.
- (24) Senn, H. M.; Thiel, W. QM/MM methods for biomolecular systems. *Angew. Chem., Int. Ed.* **2009**, *48*, 1198–1229.
- (25) Meng, S.; Wang, E. G.; Gao, S. W. Water adsorption on metal surfaces: A general picture from density functional theory studies. *Phys. Rev. B* **2004**, *69*, 195404.
- (26) Torrie, G. M.; Valleau, J. P. Nonphysical sampling distributions in Monte Carlo free-energy estimation: Umbrella sampling. *J. Comput. Phys.* **1977**, *23*, 187–199.
- (27) Straatsma, T. P.; Berendsen, H. J. C. Free energy of ionic hydration: Analysis of a thermodynamic integration technique to evaluate free energy differences by molecular dynamics simulations. *J. Chem. Phys.* **1988**, *89*, 5876–5886.
- (28) Riccardi, D.; Schaefer, P.; Yang, Y.; Yu, H. B.; Ghosh, N.; Prat-Resina, X.; Konig, P.; Li, G. H.; Xu, D. G.; Guo, H.; Elstner, M.; Cui, Q. Development of effective quantum mechanical/molecular mechanical (QM/MM) methods for complex biological processes. *J. Phys. Chem. B* **2006**, *110*, 6458–6469.
- (29) Kastner, J.; Senn, H. M.; Thiel, S.; Otte, N.; Thiel, W. QM/MM free-energy perturbation compared to thermodynamic integration and umbrella sampling: Application to an enzymatic reaction. *J. Chem. Theory Comput.* **2006**, *2*, 452–461.
- (30) Hu, H.; Yang, W. T. Free energies of chemical reactions in solution and in enzymes with ab initio quantum mechanics/molecular mechanics methods. *Annu. Rev. Phys. Chem.* **2008**, *59*, 573–601.
- (31) Zwanzig, R. W. High-temperature equation of state by a perturbation method. 1. Nonpolar gases. *J. Chem. Phys.* **1954**, *22*, 1420–1426.
- (32) Senn, H. M.; Thiel, W. QM/MM methods for biological systems. *Top. Curr. Chem.* **2007**, *268*, 173–290.
- (33) Field, M. J.; Bash, P. A.; Karplus, M. A combined quantum mechanical and molecular mechanical potential for molecular dynamics simulations. *J. Comput. Chem.* **1990**, *11*, 700–733.
- (34) Zhang, Y. K.; Lee, T. S.; Yang, W. T. A pseudobond approach to combining quantum mechanical and molecular mechanical methods. *J. Chem. Phys.* **1999**, *110*, 46–54.
- (35) Murphy, R. B.; Philipp, D. M.; Friesner, R. A. Frozen orbital QM/MM methods for density functional theory. *Chem. Phys. Lett.* **2000**, *321*, 113–120.
- (36) Lu, Z. Y.; Yang, W. T. Reaction path potential for complex systems derived from combined ab initio quantum mechanical and molecular mechanical calculations. *J. Chem. Phys.* **2004**, *121*, 89–100.
- (37) Hu, H.; Lu, Z. Y.; Yang, W. T. QM/MM minimum free-energy path: Methodology and application to triosephosphate isomerase. *J. Chem. Theory Comput.* **2007**, *3*, 390–406.
- (38) Hu, H.; Lu, Z. Y.; Parks, J. M.; Burger, S. K.; Yang, W. T. Quantum mechanics/molecular mechanics minimum free-energy path for accurate reaction energetics in solution and enzymes: Sequential sampling and optimization on the potential of mean force surface. *J. Chem. Phys.* **2008**, *128*, 034105.
- (39) Hu, H.; Yang, W. T. Development and application of ab initio QM/MM methods for mechanistic simulation of reactions in solution and in enzymes. *J. Mol. Struct.: THEOCHEM* **2009**, *898*, 17–30.
- (40) Kresse, G.; Furthmüller, J. Efficiency of ab-initio total energy calculations for metals and semiconductors using a plane-wave basis set. *Comput. Mater. Sci.* **1996**, *6*, 15–50.
- (41) Kresse, G.; Furthmüller, J. Efficient iterative schemes for ab initio total-energy calculations using a plane-wave basis set. *Phys. Rev. B* **1996**, *54*, 11169–11186.
- (42) Kresse, G.; Joubert, D. From ultrasoft pseudopotentials to the projector augmented-wave method. *Phys. Rev. B* **1999**, *59*, 1758–1775.
- (43) Perdew, J. P.; Burke, K.; Ernzerhof, M. Generalized gradient approximation made simple. *Phys. Rev. Lett.* **1996**, *77*, 3865–3868.
- (44) Perdew, J. P.; Burke, K.; Ernzerhof, M. Generalized gradient approximation made simple [Phys. Rev. Lett. *77*, 3865, (1996)]. *Phys. Rev. Lett.* **1997**, *78*, 1396–1396 Erratum.
- (45) Monkhorst, H. J.; Pack, J. D. Special points for Brillouin-zone integrations. *Phys. Rev. B* **1976**, *13*, 5188–5192.
- (46) Makov, G.; Payne, M. C. Periodic boundary conditions in ab initio calculations. *Phys. Rev. B* **1995**, *51*, 4014–4022.
- (47) Methfessel, M.; Paxton, A. T. High-precision sampling for Brillouin-zone integration in metals. *Phys. Rev. B* **1989**, *40*, 3616–3621.
- (48) Henkelman, G.; Uberuaga, B. P.; Jonsson, H. A climbing image nudged elastic band method for finding saddle points and minimum energy paths. *J. Chem. Phys.* **2000**, *113*, 9901–9904.
- (49) Henkelman, G.; Jonsson, H. Improved tangent estimate in the nudged elastic band method for finding minimum energy paths and saddle points. *J. Chem. Phys.* **2000**, *113*, 9978–9985.
- (50) Henkelman, G.; Jonsson, H. A dimer method for finding saddle points on high dimensional potential surfaces using only first derivatives. *J. Chem. Phys.* **1999**, *111*, 7010–7022.
- (51) Heyden, A.; Bell, A. T.; Keil, F. J. Efficient methods for finding transition states in chemical reactions: Comparison of improved dimer method and partitioned rational function optimization method. *J. Chem. Phys.* **2005**, *123*, 224101.
- (52) TURBOMOLE V6.4 2012, a development of University of Karlsruhe and Forschungszentrum Karlsruhe GmbH, 1989–2007, TURBOMOLE GmbH, since 2007.
- (53) Ahlrichs, R.; Bar, M.; Haser, M.; Horn, H.; Kolmel, C. Electronic structure calculations on workstation computers: The program system TURBOMOLE. *Chem. Phys. Lett.* **1989**, *162*, 165–169.
- (54) Treutler, O.; Ahlrichs, R. Efficient molecular numerical integration schemes. *J. Chem. Phys.* **1995**, *102*, 346–354.
- (55) Von Arnim, M.; Ahlrichs, R. Performance of parallel TURBOMOLE for density functional calculations. *J. Comput. Chem.* **1998**, *19*, 1746–1757.
- (56) Schafer, A.; Horn, H.; Ahlrichs, R. Fully optimized contracted Gaussian basis sets for atoms Li to Kr. *J. Chem. Phys.* **1992**, *97*, 2571–2577.

- (57) Schafer, A.; Huber, C.; Ahlrichs, R. Fully optimized contracted Gaussian basis sets of triple- ζ valence quality for atoms Li to Kr. *J. Chem. Phys.* **1994**, *100*, 5829–5835.
- (58) Eichkorn, K.; Weigend, F.; Treutler, O.; Ahlrichs, R. Auxiliary basis sets for main row atoms and transition metals and their use to approximate Coulomb potentials. *Theor. Chem. Acc.* **1997**, *97*, 119–124.
- (59) Weigend, F.; Ahlrichs, R. Balanced basis sets of split valence, triple- ζ valence and quadruple- ζ valence quality for H to Rn: Design and assessment of accuracy. *Phys. Chem. Chem. Phys.* **2005**, *7*, 3297–3305.
- (60) Eichkorn, K.; Treutler, O.; Ohm, H.; Haser, M.; Ahlrichs, R. Auxiliary basis sets to approximate Coulomb potentials. *Chem. Phys. Lett.* **1995**, *240*, 283–289.
- (61) Weigend, F. Accurate Coulomb-fitting basis sets for H to Rn. *Phys. Chem. Chem. Phys.* **2006**, *8*, 1057–1065.
- (62) Klamt, A.; Jonas, V. Treatment of the outlying charge in continuum solvation models. *J. Chem. Phys.* **1996**, *105*, 9972–9981.
- (63) Schafer, A.; Klamt, A.; Sattel, D.; Lohrenz, J. C. W.; Eckert, F. COSMO implementation in TURBOMOLE: Extension of an efficient quantum chemical code towards liquid systems. *Phys. Chem. Chem. Phys.* **2000**, *2*, 2187–2193.
- (64) Klamt, A. Conductor-like screening model for real solvents: A new approach to the quantitative calculation of solvation phenomena. *J. Phys. Chem.* **1995**, *99*, 2224–2235.
- (65) Klamt, A.; Jonas, V.; Burger, T.; Lohrenz, J. C. W. Refinement and parametrization of COSMO-RS. *J. Phys. Chem. A* **1998**, *102*, 5074–5085.
- (66) Klamt, A. *COSMO-RS: From Quantum Chemistry to Fluid Phase Thermodynamics and Drug Design*; Elsevier Science Ltd.: Amsterdam, The Netherlands, 2005.
- (67) Perdew, J. P. Density-functional approximation for the correlation energy of the inhomogeneous electron gas. *Phys. Rev. B* **1986**, *33*, 8822–8824.
- (68) Becke, A. D. Density-functional exchange-energy approximation with correct asymptotic behavior. *Phys. Rev. A* **1988**, *38*, 3098–3100.
- (69) Burow, A. M.; Sierka, M.; Dobler, J.; Sauer, J. Point defects in CaF₂ and CeO₂ investigated by the periodic electrostatic embedded cluster method. *J. Chem. Phys.* **2009**, *130*, 174710.
- (70) Jorgensen, W. L.; Chandrasekhar, J.; Madura, J. D.; Impey, R. W.; Klein, M. L. Comparison of simple potential functions for simulating liquid water. *J. Chem. Phys.* **1983**, *79*, 926–935.
- (71) Reed, A. E.; Weinstock, R. B.; Weinhold, F. Natural population analysis. *J. Chem. Phys.* **1985**, *83*, 735–746.
- (72) See Supporting Information for comparison of invariability and computational cost of ESP-fitted and NPA charges.
- (73) Todorov, I. T.; Smith, W.; Trachenko, K.; Dove, M. T. DL_POLY_3: New dimensions in molecular dynamics simulations via massive parallelism. *J. Mater. Chem.* **2006**, *16*, 1911–1918.
- (74) Smith, W.; Forester, T. R. Parallel macromolecular simulations and the replicated data strategy. 2. The RD-SHAKE algorithm. *Comput. Phys. Commun.* **1994**, *79*, 63–77.
- (75) Berendsen, H. J. C.; Postma, J. P. M.; Vangunsteren, W. F.; Dinola, A.; Haak, J. R. Molecular dynamics with coupling to an external bath. *J. Chem. Phys.* **1984**, *81*, 3684–3690.
- (76) Essmann, U.; Perera, L.; Berkowitz, M. L.; Darden, T.; Lee, H.; Pedersen, L. G. A smooth particle mesh Ewald method. *J. Chem. Phys.* **1995**, *103*, 8577–8593.
- (77) Spohr, E. Computer simulation of the water/platinum interface. *J. Phys. Chem.* **1989**, *93*, 6171–6180.
- (78) Jorgensen, W. L. Optimized intermolecular potential functions for liquid alcohols. *J. Phys. Chem.* **1986**, *90*, 1276–1284.
- (79) Geerke, D. P.; Van Gunsteren, W. F. The performance of non-polarizable and polarizable force-field parameter sets for ethylene glycol in molecular dynamics simulations of the pure liquid and its aqueous mixtures. *Mol. Phys.* **2007**, *105*, 1861–1881.